Publ. Astron. Soc. Japan (2020) 72 (2), L4 (1–6)
doi: 10.1093/pasj/psaa011
Advance Access Publication Date: 2020 March 9
Letter

Letter

Galactic Center threads as nuclear magnetohydrodynamic waves

Yoshiaki SOFUE*

Institute of Astronomy, The University of Tokyo, 2-21-1 Osawa, Mitaka, Tokyo 181-0015, Japan

*E-mail: sofue@ioa.s.u-tokyo.ac.jp

Received 2019 November 6; Accepted 2020 January 31

Abstract

Propagation of fast-mode magnetohydrodynamic (MHD) compression waves is traced in the Galactic Center with a poloidal magnetic cylinder. MHD waves ejected from the nucleus are reflected and guided along the magnetic field, exhibiting vertically stretched fronts. The radio threads and non-thermal filaments are explained as due to tangential views of the waves driven by sporadic activity in Sgr A*, or by multiple supernovae. In the latter case, the threads could be extremely deformed relics of old supernova remnants exploded in the nucleus.

Key words: galaxies: individual (Galactic Center) — galaxies: nucleus — ISM: magnetic field — magnetohydrodynamics (MHD)

1 Introduction

Non-thermal filaments (NTF) and radio continuum threads (hereafter, threads) in the Galactic Center (GC) are unique for their straight and narrow morphology perpendicular to the galactic plane (Yusef-Zadeh et al. 1984, 2004; Morris & Yusef-Zadeh 1985; Tsuboi et al. 1986; Anantharamaiah et al. 1991; Lang et al. 1999a, 1999b; LaRosa et al. 2004). The wide-field image of the GC at 1.3 GHz with the MeerKAT radio telescope (Heywood et al. 2019) has revealed a large-scale poloidal magnetic structure composed of coherently aligned vertical threads, which penetrate through the central molecular zone (CMZ: Oka et al. 1998, 2012; Tsuboi et al. 2015). On the other hand, high-latitude threads are well correlated with the side edges of the Galactic Center Lobe (GCL: Sofue & Handa 1984; Sofue 1985), which is one of the typical emerging phenomena commonly observed in the nuclei of disk galaxies.

There have been several ideas to explain the unique properties of threads and their physical relation to the central disk and nuclear activity (Sofue & Fujimoto 1987; Dahlburg et al. 2002; Boldyrev & Yusef-Zadeh 2006; Yusef-Zadeh & Wardle 2019; Barkov & Lyutikov 2019). However, the mechanism to explain the straight vertical structures coherently penetrating the disk appears still unresolved. In this paper we propose a new mechanism for the origin of the threads based on a simulation of the propagation of magnetohydrodynamic (MHD) waves excited by the activity of Sgr A* and supernovae around the nucleus.

2 MHD waves and thread formation

Disturbances excited by explosive events in the nucleus propagate as a spherical shock wave in the initial phase. In the fully expanded phase, they propagate as sound, Alfvén, and fast-mode MHD waves of small amplitudes. The Alfvén wave transports energy along the field lines, while it does not compress the local field. The fast-mode MHD wave (hereafter, MHD wave) propagates across the magnetic field lines at the Alfvén velocity and compresses

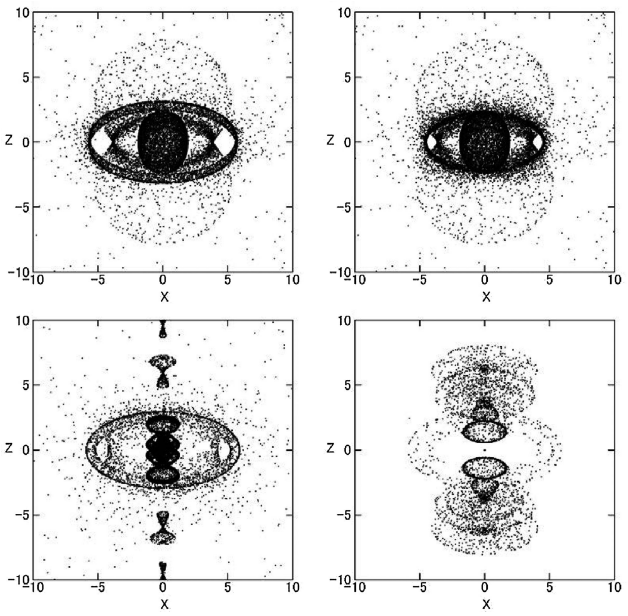

Fig. 1. MHD wave fronts every $\delta t = 2$ seen from 30° above the galactic plane through: (top left) sech disk with $h = 1$: waves make bipolar shells and converge onto a focal ring of radius 4.4; (top right) same as the top left panel + gas ring of radius 5: waves converge to the ring more efficiently; (bottom left) same as top right panel + magnetic cylinder of radius 3: waves are guided by the cylinder; (bottom right) same as bottom left panel, but open magnetic cylinder: waves are guided by the cylinder, but are more diverged and make bipolar caps.

the local field, leading to enhanced synchrotron emission. The propagation of MHD waves originating at the nucleus is traced by solving the Eikonal equations developed by Uchida (1970, 1974), which have been also applied to the GC (Sofue 1977, 1980). The equations are solved for a given distribution of Alfvén velocity $V = \sqrt{B^2/4\pi\rho}$.

We assume that the non-dimensionalized gas density is expressed by superposition of three components: (i) a plane-parallel disk with density distribution $\rho_{\rm disk} = {\rm sech}(z/h)$, where $h = 1$ is the scale height; (ii) a molecular ring representing the CMZ, $\rho_{\rm ring} = 10\, e^{-[(r-r_{\rm ring})^2+z^2]/w^2_{\rm ring}}$, where $r_{\rm ring} = 5$ and $w_{\rm ring} = 0.5$ are the radius and width of the ring; and (iii) a low-density halo with $\rho_{\rm halo} = 0.1$.

The distribution of magnetic strength is expressed by an offset, oblique, and open cylindrical form: $B = [1. + \beta e^{-\{[r(x,y,z)-r_{\rm m}]/w_{\rm m}\}^2}][1. + (z/z_{\rm m})^2]^{-1}$, where $r(x, y, z) = [(x - 0.5 - 0.2z)^2 + (y - 0.1z)^2]^{1/2}$, $r_{\rm m} = 3\{1 + 2(z/z_{\rm m})^2/[1 + (z/z_{\rm m})^2]\}$, and β is a parameter to represent the magnetic strength, which is taken to be $\sim$10, $w_{\rm m} = 1$, and $z_{\rm m} = 3$. Here, (x, y, z) are the Cartesian coordinates with z being the polar axis, and $r_{\rm m}$, $w_{\rm m}$, and $z_{\rm m}$ are the radius, width, and vertical scale of variation of radius of the cylinder, respectively.

The real quantities are obtained using the units of length A, time $t_{\rm unit}$, and velocity $V_{\rm unit} = B_{\rm unit}/\sqrt{4\pi\rho_{\rm unit}}$, and the following values are assumed: $\rho_{\rm unit} = 100\,{\rm H\,cm^{-3}}$, $B_{\rm unit} = 1\,{\rm mG}$, $A = 20\,{\rm pc}$, leading to $V_{\rm unit} = B_{\rm unit}/\sqrt{4\pi\rho_{\rm unit}} = 219\,{\rm km\,s^{-1}}$ and $t_{\rm unit} = 0.0898\,{\rm Myr}$ ($\sim 10^5\,{\rm yr}$). The Alfvén velocity is calculated to be $V_{\rm A} \sim 20\,{\rm km\,s^{-1}}$ in the molecular ring and $\sim$200 km s^{-1} in the galactic disk, which are higher than the sound velocities of the molecular ($c_{\rm s} \sim 0.1$–$0.2\,{\rm km\,s^{-1}}$) and HI ($\sim 1\,{\rm km\,s^{-1}}$) gases. In the halo, $V_{\rm A}$ increases rapidly, due to the decreasing gas density, to $\sim 10^3\,{\rm km\,s^{-1}}$ or even higher in the magnetic cylinder, and is also higher than the $c_{\rm s} \sim 100\,{\rm km\,s^{-1}}$ of the hot halo gas. In the present model, the entire region is thus assumed to be magnetically dominated, so that the Eikonal method can be safely applied.

The top left panel of figure 1 shows the result for a disk and halo with constant B. According to the rapid increase of V toward the halo, the waves are strongly reflected and focus on a ring of radius $f_{\rm ring} \sim 4.4\,h$. Here, the disk plays the role of a convex lens with a focal length of $f_{\rm disk} = 2.2\,h$ for a plane wave (Sofue 1977). The top right panel is the case when a gas ring of radius $r_{\rm ring} = 5$ is added to the disk, where the Alfvén velocity is lower than in the disk. The waves focus on and are trapped by the gas ring. Figure 1 (bottom left) shows the case when a straight vertical magnetic cylinder is added. The waves are strongly reflected by the inner wall of the cylinder and are channeled along the polar axis. Some fraction of the waves penetrate the cylinder and are trapped by the gas ring. The bottom right panel shows the same, but the magnetic cylinder is open toward the halo. The waves are accordingly more open and make bipolar caps.

In order to simulate a more realistic case in the GC, an open, oblique, and offset magnetic cylinder is added to the disk and ring, and the result is shown in figure 2. The left half is reflected by the nearside inner wall of the cylinder, and expands backward toward the other side. It then merges with the original half, and both are guided along the cylinder to result in bipolar channeled MHD waves. The front finally makes a vertically stretched and corrugated sheet near the disk and bipolar caps in the halo. Figure 3 enlarges the central region at $t = 2$–4, 4–6, and 6–8. Note that the figure does not represent the radio brightness, which is much suppressed at high latitudes and in horizontal threads (see subsection 3.3 for the radio emission).

Figure 4 shows the fronts from $t = 3$ to 8 at a smaller interval of 0.5, and compares them with the observation at 1.3 GHz (Heywood et al. 2019). The tangential projection of the MHD front sheets mimic well the observed radio threads. Parallel magnetic orientation in isolated threads (Lang et al. 1999a) may be understood as due to the projected view of compressed field lines in the fronts. Again, see subsection 3.3 for the radio emission.

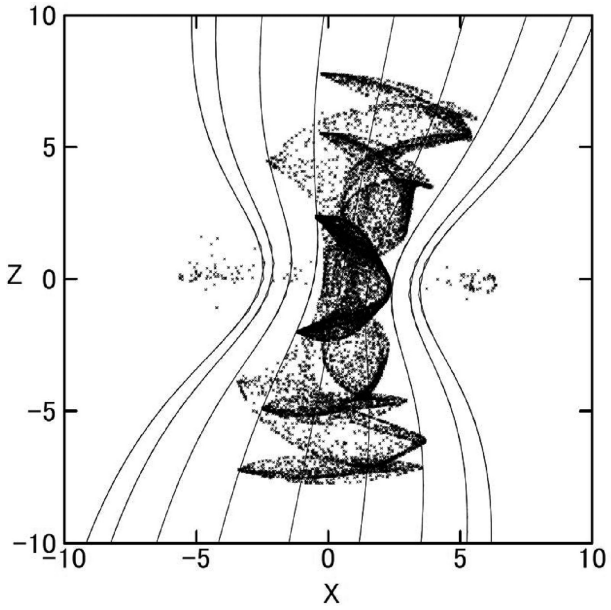

Fig. 2. MHD wave fronts seen from the galactic plane in an offset, open, and oblique magnetic cylinder as drawn by the lines schematically. Waves are bent, deformed, and stretched in the *z* direction, while both top fronts make bipolar caps.

3 Discussion

3.1 Poloidal magnetic field

It has been shown that a nuclear poloidal field is created by secular accumulation of an intergalactic magnetic field frozen into a forming galaxy (Sofue & Fujimoto 1987; Sofue et al. 2010). Since the vertical component can neither escape across the accreting disk nor be dissipated because of the absence of a neutral sheet, they are secularly concentrated onto the GC and form a strong vertical flux (figure 5; Sofue & Fujimoto 1987). The model is in accordance with the radio continuum observations of the well-ordered poloidal magnetic structure penetrating the GC disk without twisting (Heywood et al. 2019).

The vertical field is maximized in a cylinder around the polar axis, being sandwiched between the accumulating flux from outside and high pressure from inside by the hot nuclear gas (Nakashima et al. 2019; Ponti et al. 2019). Since the magnetic field is anchored to intergalactic space at rest, the accumulated field will also be at rest when it becomes stationary after a cosmic time. This means that the field lines run through the cavity inside the CMZ's ring without rotation.

If the magnetic field were not rotating, the frozen-in gas would also be at rest, which has indeed been confirmed by the recent observation of slow or almost no rotation of the GCL using the H92α recombination line (Nagoshi et al. 2019). The coherently aligned, straight, and non-twisted morphology indicates that the threads are not interacting

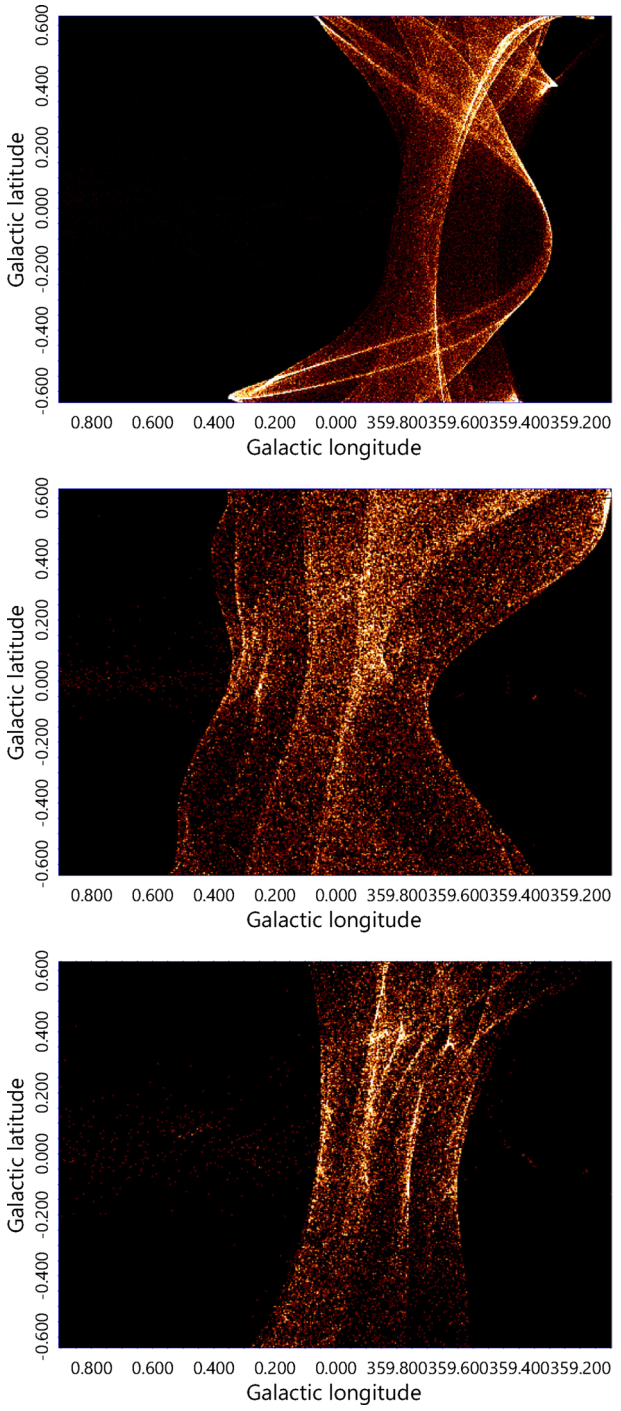

Fig. 3. MHD waves in an oblique, open, and offset magnetic cylinder at (top) $t = 2$–4, (middle) 4–6, and (bottom) 6–8, exhibiting thread features as tangential projections of the wave fronts. Note that the figure does not represent the radio brightness. The radio emission is suppressed at high latitudes and in horizontal threads (see subsection 3.3 for the radio emission). (Color online)

with the rotating gas disc. The threads are further continued by an even longer radio spur at 2.7 GHz reaching to $z \sim -350$ pc (Reich et al. 1984). All these facts suggest that the threads are a part of a structure at rest continued from the intergalactic space.

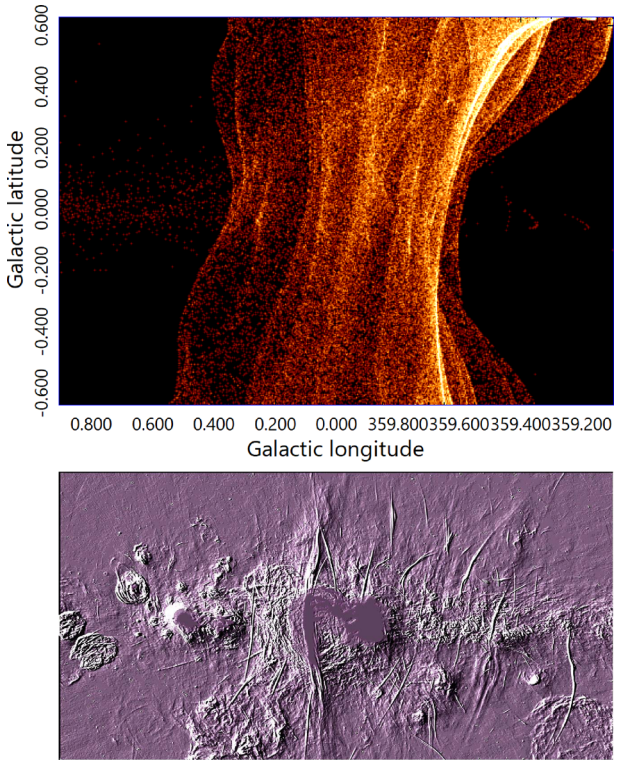

Fig. 4. Projection of three-dimensional MHD wave fronts on the sky at $t =$ 3 to 8 by interval $\delta t = 0.5$ (for the radio emission, see subsection 3.3). The bottom panel shows a 1.3 GHz radio image taken from the web page of NASA (⟨*https://apod.nasa.gov/apod/ap190708.html*⟩, credit: MeerKAT, SARAO) (Heywood et al. 2019). Threads are enhanced in relief. (Color online)

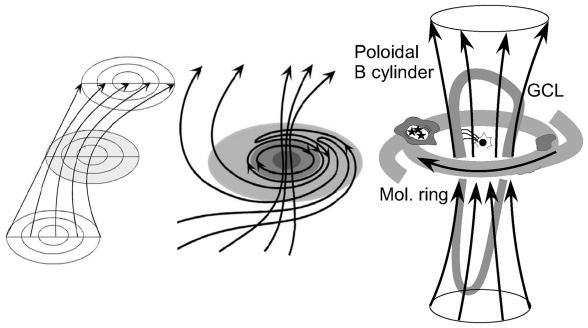

Fig. 5. Formation of poloidal magnetic field in the GC, ring, and spiral fields in the disk (Sofue & Fujimoto 1987; Sofue et al. 2010). The right panel illustrates the GCL, molecular ring (CMZ), and supposed poloidal field in the GC.

3.2 Proper motion

Although the magnetic field is at rest, threads are moving at the Alfvén velocity of the order of $\sim$200 km s^{-1} at random, so at mutual random velocities of $\sim$400 km s^{-1}. This would cause proper motions between neighboring or overlapping threads on the order of $\sim$10 mas yr^{-1}. On the contrary, if the magnetic field is rotating with the disk, and the filaments are thin magnetic fluxes, the threads' proper motion would be more systematic in that the mutual proper motion decreases with the distance from the rotation axis.

3.3 Magnetic strength and radio brightness

Let Δ be the thickness of an MHD wave front and R the curvature. Then the tangential line-of-sight depth is given by $\Lambda_{\rm wave} = \sqrt{2R\Delta}$. If we assume $R \sim 30$ pc and $\Delta \sim 0.04$ pc ($1''$) as for the thinnest thread (Paré et al. 2019), we obtain $\Lambda_{\rm wave} \sim 1.5$ pc. On the other hand, if the thread is a string, the depth would be about the same as its diameter, $\Lambda_{\rm string} \sim \Delta \sim 0.04$ pc. Then, the emissivity to obtain the observed radio brightness for the MHD wave model being that for the string model can be minimized by a factor of $\kappa = \epsilon_{wave}/\epsilon_{\rm string} = L_{\rm string}/L_{\rm wave} \sim 0.03$.

Assuming the energy equipartition for a volume emissivity $\epsilon \sim \nu\Sigma_\nu/\Lambda$, where $\Sigma_\nu \sim 80$ mJy beam^{-1} by a $\sim 1''$ beam at $\nu = 10$ GHz (Paré et al. 2019) and measured thread width of $\sim 1''$, the magnetic strength is estimated to be $B \sim 0.6$ mG in the string model, and $B \sim 0.2$ mG in the wave model. The wave model can, thus, save the energy by an order of magnitude compared to the string model.

The radio emissivity, and hence the brightness Σ, varies with B as well as with the angle between the directions of wave propagation and the field, θ. We may then approximate the variation of synchrotron brightness as $\Sigma \propto (B_\perp)^{3.5} \sim (B\sin\theta)^{3.5} \propto \{[1 + (z/z_{\rm m})^2]\sin\theta\}^{-3.5}$. A model radio map may be obtained by multiplying this factor to the front's projected density maps. This results in a more rapidly decreasing radio brightness with latitude and suppressed emission for horizontal features. The larger number of brighter threads near the galactic plane may be understood by such latitudinal as well as the θ variation of the emissivity.

3.4 Dissipation and heating of the GCL

Neglecting the Ohmic loss, the dissipation rate γ of the MHD wave (Landau & Lifshitz 1960) is given by $\gamma = \omega^2\nu_{\rm d}/(2V^3\rho)$, where $\omega = 2\pi V/\lambda$ is the frequency and $\nu_{\rm d}$ is the viscosity of hydrogen gas. The dissipation length, $D = 1/\gamma$, is then estimated by $(D/pc) \sim 570(B/\mu{\rm G})(\rho/{\rm H\,cm^{-3}})^{1/2}(\nu_{\rm d}/10^{-4}\,{\rm g\,cm\,s^{-1}})^{-1}(\lambda/{\rm pc})^2$. This yields a sufficiently long distance, $D \sim 5$ kpc, near the galactic disk for $B \sim 1$ mG and $\rho \sim 100\,{\rm H\,cm^{-3}}$, and the wave is dissipation less.

On the other hand, outside the disk with less density and magnetic field as $B \sim 0.1$ mG and $\rho \sim 1\,{\rm H\,cm^{-3}}$, the wave is dissipated in $D \sim 50$ pc, and thermalized to heat the gas inside the magnetic cylinder. According to the decrease in the gas density and magnetic strength, the wave amplitude will increase with the height from the Galactic plane, and

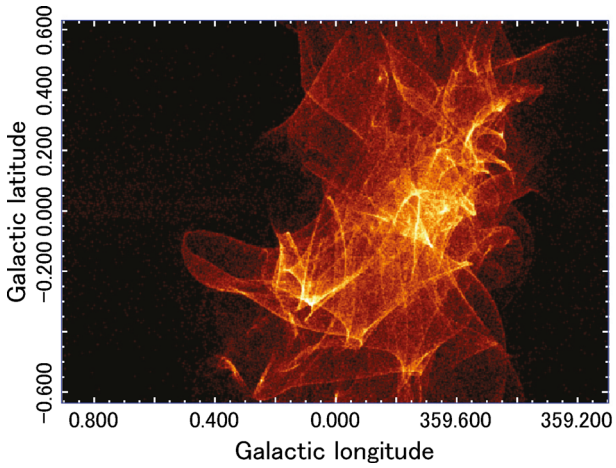

Fig. 6. MHD wave fronts in an offset and oblique straight magnetic cylinder through a gas disk with tight concentration to the plane, resulting in strong confinement near the plane and complicated structures. Note, however, that the synchrotron radio brightness of the wave front decreases with the latitude more rapidly and horizontal features are much suppressed (see subsection 3.3). (Color online)

at some height they will be rapidly dissipated to heat the surrounding gas.

It should also be mentioned that a comparable fraction of the energy released in the nucleus is transported in the form of Alfvén velocity in the polar direction along the vertical magnetic fields. According to the rapid decrease in the halo gas density, the wave amplitude will increase, and attain non-linear growth at a certain height, where the waves will be dissipated to heat the GCL.

Such heating of the halo gas due to MHD- and Alfvén-wave dissipation as well as accumulation of the wave flux at high latitudes would become a heating source of the GCL, which is observed to be filled with ionized hydrogen gas (Sofue 1985; Nagoshi et al. 2019).

3.5 Unique morphology

The present model reproduces well not only the straight filaments, but also those with peculiar morphology in the Arc (Paré et al. 2019) and horizontal threads (Lang et al. 1999b): bifurcated and crossed threads are due to the projection of two or multiple fronts ejected at different epochs and/or those superposed by retarded reflections. Double and multiple strings are also explained by such multiple fronts. Threads having kinks, bends, and bright knots, and maybe mouse-like spots, can be explained by superposition of obliquely corrugated and warped MHD fronts. Figure 6 shows an example of a simulation in a straight and offset magnetic cylinder and a disk with smaller scale height, where the increase of Alfvén velocity is steeper, so that the reflection is stronger. The waves are confined near the origin, and exhibit a variety of filamentary structures.

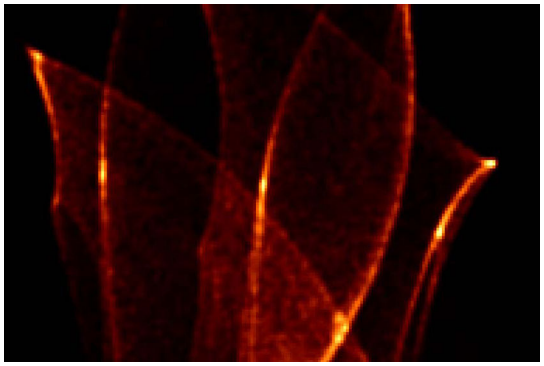

Fig. 7. Enlargement of a portion of the MHD waves, showing bifurcation, kink, bend, mice, and crossed threads. (Color online)

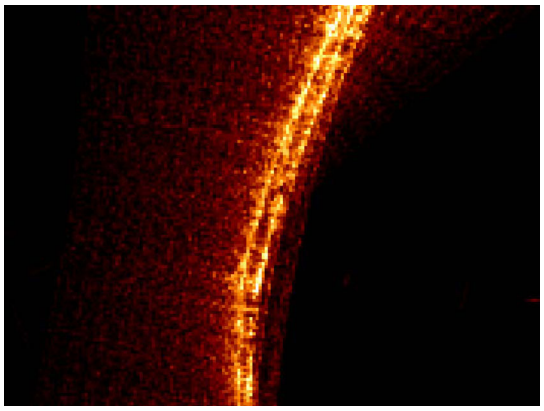

Fig. 8. Enlargement of a portion of the MHD waves at $t = 3$ to 4 by an interval of $\delta t = 0.1$, mimicking the NTF in the Arc. Faint horizontal waves are superposed, making the threads apparently clumpy. (Color online)

Figure 7 enlarges part of the simulation, showing crossed and horizontal threads as well.

The bunched NTF in the radio Arc (Yusef-Zadeh et al. 1984) could be due to a past temporal enhancement of activity associated with multiple disturbances at a shorter time interval. Figure 8 shows an enlarged portion of the simulated waves from $t = 3$ to 4 at an interval of $\delta t = 0.1$, where the tangential projection of the fronts resembles the observed NTF in the Arc. It is stressed that the threads show apparently clumpy features due to superposition of horizontal and fainter waves in the fore- and backgrounds, which is indeed observed (Paré et al. 2019).

3.6 Time variation in Sgr A

Sporadic arrival of the waves produces multiple threads, whose spatial interval manifests the time interval of the ejections as $\delta L \sim V\delta t$. The interval between the brightest threads is observed to be $\delta L \sim 20\,\mathrm{pc}$ (e.g. Anantharamaiah et al. 1991), which corresponds to a time interval of $\delta t \sim 10^5\,\mathrm{yr}$ for $V \sim 200\,\mathrm{km\,s^{-1}}$. This time may be compared with those suggested for the GCL (∼0.1 Myr), Fermi

bubbles (FB: ∼1 Myr), and the bipolar hypershells (BHS: ∼10 Myr)—see Kataoka et al. (2018) for a review.

Numerous minor threads at intervals of $\delta L \sim 2$ pc (Heywood et al. 2019; Paré et al. 2019) may correspond to waves emitted in shorter time scales of $\sim 10^4$ yr. Furthermore, much shorter intervals and fainter threads may exist according to less energetic and shorter-time activity as observed as the time variation of Sgr A* (Subroweit et al. 2017). Such weak waves could be observed as numerous faint threads with sub- to milli-pc intervals.

3.7 Possible origin of the threads and energetics

The magnetic energy contained in a single thread is estimated to be $E \sim B^2/(8\pi)4\pi R^2 \Delta \sim 10^{50}$ erg for an assumed magnetic strength of $B \sim 0.3$ mG (log mean of 0.1 to 1 mG) with $R \sim 30$ pc and $\Delta \sim 0.04$ pc. Namely, about 10% of the released kinetic energy by a single core-collapse supernova (SN; 10^{51} erg) is sufficient to drive one thread. This energetic proximity might indicate that a thread is an extremely deformed relic of an old supernova remnant (SNR). Namely, the presently observed threads might be an ensemble of such old SNRs due to bursting SNe in the nucleus some 10^5 yr ago. Alternatively, the energy source could be sporadic puffing activity of Sgr A*. This idea applies particularly to numerous fainter threads, which may be waves driven by less energetic activities in the nucleus with shorter time scales. In either case, the total energy to drive all the observed threads is on the order of $\sim 10^{52}$ erg. Or, only a small fraction of the energy required for GC bubbles like GCL, FB, and BHS (10^{54}–10^{55} erg) will be sufficient to produce the GC threads.

4 Summary

Propagation of fast-mode MHD compression waves was traced in the GC penetrated by an open, off-axis, and oblique poloidal magnetic field. Reflected and guided waves exhibit vertically stretched fronts, and their tangential projections well mimic the morphological properties of radio threads and non-thermal filaments. The origin of the poloidal field is explained as due to secular accumulation of frozen-in primordial magnetic fields to the Galaxy. Energetics suggests that the MHD waves are due either to sporadic puffing in Sgr A* or to multiple SNe some 10^5 yr ago. In the latter case, the threads may be regarded as an ensemble of extremely deformed relics of old supernova remnants exploded in the nucleus.

Acknowledgments

Computations were carried out at the Astronomy Data Center of the National Astronomical Observatory of Japan.

References

Anantharamaiah, K. R., Pedlar, A., Ekers, R. D., & Goss, W. M. 1991, MNRAS, 249, 262
Barkov, M. V., & Lyutikov, M. 2019, MNRAS, 489, L28
Boldyrev, S., & Yusef-Zadeh, F. 2006, ApJ, 637, L101
Dahlburg, R. B., Einaudi, G., LaRosa, T. N., & Shore, S. N. 2002, ApJ, 568, 220
Heywood, I., et al. 2019, Nature, 573, 235
Kataoka, J., Sofue, Y., Inoue, Y., Akita, M., Nakashima, S., & Totani, T. 2018, Galaxies, 6, 27
Landau, L. D., & Lifshitz, E. M. 1960, Electrodynamics of Continuous Media (Oxford: Pergamon Press), ch. VIII
Lang, C. C., Anantharamaiah, K. R., Kassim, N. E., & Lazio, T. J. W. 1999a, ApJ, 521, L41
Lang, C. C., Morris, M., & Echevarria, L. 1999b, ApJ, 526, 727
LaRosa, T. N., Nord, M. E., Lazio, T. J. W., & Kassim, N. E. 2004, ApJ, 607, 302
Morris, M., & Yusef-Zadeh, F. 1985, AJ, 90, 2511
Nagoshi, H., et al. 2019, PASJ, 71, 80
Nakashima, S., Koyama, K., Wang, Q. D., & Enokiya, R. 2019, ApJ, 875, 32
Oka, T., Hasegawa, T., Sato, F., Tsuboi, M., & Miyazaki, A. 1998, ApJS, 118, 455
Oka, T., Onodera, Y., Nagai, M., Tanaka, K., Matsumura, S., & Kamegai, K. 2012, ApJS, 201, 14
Paré, D. M., Lang, C. C., Morris, M. R., Moore, H., & Mao, S. A. 2019, ApJ, 884, 170
Ponti, G., et al. 2019, Nature, 567, 347
Reich, W., Fuerst, E., Haslam, C. G. T., Steffen, P., & Reif, K. 1984, A&AS, 58, 197
Sofue, Y. 1977, A&A, 60, 327
Sofue, Y. 1980, PASJ, 32, 79
Sofue, Y. 1985, PASJ, 37, 697
Sofue, Y., & Fujimoto, M. 1987, PASJ, 39, 843
Sofue, Y., & Handa, T. 1984, Nature, 310, 568
Sofue, Y., Machida, M., & Kudoh, T. 2010, PASJ, 62, 1191
Subroweit, M., García-Marín, M., Eckart, A., Borkar, A., Valencia-S., M., Witzel, G., Shahzamanian, B., & Straubmeier, C. 2017, A&A, 601, A80
Tsuboi, M., Inoue, M., Handa, T., Tabara, H., Kato, T., Sofue, Y., & Kaifu, N. 1986, AJ, 92, 818
Tsuboi, M., Miyazaki, A., & Uehara, K. 2015, PASJ, 67, 90
Uchida, Y. 1970, PASJ, 22, 341
Uchida, Y. 1974, Sol Phys., 39, 431
Yusef-Zadeh, F., Hewitt, J. W., & Cotton, W. 2004, ApJS, 155, 421
Yusef-Zadeh, F., Morris, M., & Chance, D. 1984, Nature, 310, 557
Yusef-Zadeh, F., & Wardle, M. 2019, MNRAS, 490, L1